Improvement of microstructure and tribological properties of titanium nitride films by optimization of substrate bias current

Qi Xie [a,b], Zhiqiang Fu [a,b,c,*], Ziyi Liu [a], Wen Yue [a,b,c], Jiajie Kang [a,b,c], Lina Zhu [a,b,c], Chengbiao Wang [b,d], Songsheng Lin [e]

[a] School of Engineering and Technology, China University of Geosciences (Beijing), Beijing 100083, China
[b] Zhengzhou Institute, China University of Geosciences (Beijing), Zhengzhou 451283, China
[c] National International Joint Research Center of Deep Geodrilling Equipment, China University of Geosciences (Beijing), Beijing 100083, China
[d] Zhengzhou Institute of Multipurpose Utilization of Mineral Resources, Chinese Academy of Geological Sciences, Zhengzhou 450006, China
[e] Institute of New Materials, Guangdong Academy of Sciences, Guangzhou 510651, China

ARTICLE INFO

ABSTRACT

Severe wear is a key factor affecting the work character and service life of the cutting tools used for dry cutting. The deposition of wear-resistant films on the cutting tools via magnetron sputtering is one of the most effective strategies, and the further improvement of the properties of the deposited films has attracted much attention. Plasma-enhanced magnetron sputtering possesses a much higher ionization rate than conventional magnetron sputtering and has been used to deposit dense hard wear-resistant film, but the influence of substrate bias current (I_s) on the structure and properties of the films should be further studied. In this paper, plasma-enhanced magnetron sputtering technique was utilized to obtain an individually adjustable I_s and TiN film was taken as an example to study the effects of I_s on the properties of the films. It is found that the microstructure of the films is transformed from a loose columnar microstructure into a dense and featureless microstructure with increasing I_s from 0.1 to 3.0 A, and the preferred growth orientation along TiN(111) is found at a high level of I_s. As I_s increases from 0.1 to 1.5 A, the grain size of the films is abruptly decreased, and the mechanical properties are significantly improved; but when I_s further increases, the mechanical properties stay nearly unchanged. When I_s is increased, the wear rate of TiN-coated samples is distinctly decreased at first, and then gradually increased. When I_s is 3.0 A, the highest hardness of 38.7 GPa and lowest wear rate of 9.4×10^{-16} m^3/(N•m) are obtained for the TiN-coated sample.

1. Introduction

Dry cutting has become a trend of development of machinery manufacturing industry for its benefits in protecting environment and reducing production cost by using no or less cutting fluid. However, due to the poor cooling and lubrication conditions in dry cutting process, the cutting tools are subjected to severe wear. The wear of cutting tools is closely related to their surface properties. Hence, many attempts have been made to improve the wear resistance of the cutting tools by surface technology. Machado et al. [1] concluded that surface texturing technique becomes a promising method for improving machinability and reducing wear in the recent decades. Besides surface texturing, Hacisalihoglu et al. [2] reported that Ti-based and Cr-based nitride films can also enhance the wear resistance of AISI M2 high speed tool steel by

more than 15 times because of their excellent mechanical properties, good thermal stability, and high wear resistance. The wear-resistant films are usually prepared by chemical vapor deposition (CVD) and physical vapor deposition (PVD) techniques. Celik et al. [3] compared the dry cutting performance of the WC tools coated with a typical CVD-TiCN/Al$_2$O$_3$/TiN multilayer film and a PVD-TiAlN film. They found that the PVD-coated WC tools show better wear-resistance than the CVD-coated WC tools. Among the PVD processes, arc ion evaporation is preferred for its inherent advantages such as high deposition and ionization rates, and has been used to deposit various nitride-based films including TiN, TiCN, TiAlN and CrN on the cutting tools in the literatures represented by Hacisalihoglu et al. [2]. However, according to the investigation conducted by Tkadletz et al. [4], the concomitant droplets induce the cracks in the films and act as abrasive medium, resulting in

increased wear. Magnetron sputtering has been widely used for depositing smooth films. And the further improvement of the structure and properties of the wear-resistant films deposited by magnetron sputtering has attracted much attention.

For magnetron sputtering technique, the properties and wear performance of the deposited films are closely dependent on the process parameters. Zhang et al. [5] reported that an obvious change of the phase structure in the CrN$_x$ films occurs by varying the fraction of N$_2$ flux in N$_2$ and Ar mixed gas. And the mechanical properties and wear performance of the CrN$_x$ films deposited by magnetron sputtering are greatly influenced by their phase composition. Biswas et al. [6] found that a relative low total pressure used for depositing CrN/NbN films benefits the reduction of surface defects and wear. Mayhofer et al. [7] systematically investigated the effect of nitrogen partial pressure, total pressure, substrate bias voltage (U_s) and ion/atom flux ratio on the microstructure, hardness, residual stress of the CrN films deposited by unbalanced magnetron sputtering. They concluded that the variation of the energy and flux of ions possesses a great impact on the microstrcutre and properties of the films. Chen et al. [8] confirmed that applying a temperate U_s is beneficial to improve the wear performance of TiN films. Jaroš et al. [9] also reported that the ion energy controlled by U_s, is a key parameter for controlling the microstructure, mechanical properties, and resistance to cracking of Ti(Al,V)N$_x$ films. According to Mayrhofer et al. [10], besides U_s, an increased substrate bias current (I_s) also causes a densifying and smoothing process during film deposition. And the compressive stress in the films induced by a high level of U_s can be released by increasing I_s. But on account of the extremely low ionization rate of the films-forming particles and gas molecules during conventional magnetron sputtering (CMS) process, it is difficult to adjust I_s to a proper level. In order to address this issue, Lin et al. [11] utilized middle frequency pulsed magnetron sputtering (MFMS) power to enhance the ionization rate and ion energy during the deposition process of CrN$_x$ films. They found that the hardness and wear resistance of the CrN$_x$ films deposited by MFMS are significantly increased, compared with those of the films synthesized by CMS. On that basis, Ma et al. [12] used high power impulse magnetron sputtering to prepare superhard TiAlSiN films on cement carbides.

Plasma-enhanced magnetron sputtering (PEMS) technique introduces an extra electron-emitting source into CMS equipment so that the plasma density around the substrates can be significantly increased. Matossian et al. [13] reported that PEMS technique is an effective and economical way to enhance the ion bombardment during magnetron sputtering process. El-Rahman and Wei [14] showed that thanking to the high plasma density, a distinctly increased and individually controllable I_s can be achieved at a relative low level of U_s. During the film deposition process, high I_s can not only clean the substrates more completely, but also enhance the ion bombardment on the forming films. Wei et al. [15] found that the service lives of the coated tools fabricated by PEMS are much longer than those of the coated tools fabricated using arc-evaporation and CMS processes. Furthermore, El-Rahman and Wei [16] obtained the superhard nanocomposite TiSiCN films with excellent erosion and corrosion resistance via opitmizing the substrate power denstiy during PEMS process. Besides Ti-based wear-resistant films, the preparation of single phase or nanocomposite Cr-based films including CrN and CrSiCN films with significantly improved compactness, mechanical properties, and wear resistance via PEMS technique was reported by Lorenzo-Martin et al. [17] and Cai et al. [18]. Although I_s plays an important role in the deposition of the films, the effect of I_s on the structure and properties of the wear-resistant nitride films deposited by PEMS is not very clear so far. Therefore, the systematical investigation of the influence of I_s on the mechanical properties and tribological behavior of the wear-resistant films is of great value to the manufacture of the high-quality films used for dry cutting tools. In this paper, TiN film, which has been widely used for improving the performance of cutting tools, was selected as a research example, to investigate the relationships between I_s and the microstructure and properties of the wear-resistant films deposited by PEMS.

2. Experimental details

TiN films were deposited on polished Si(100) wafers (20 mm × 20 mm, resistivity is less than 0.01 Ω•cm) and 40Cr13 stainless steel plates (50 mm × 30 mm × 7 mm) by PEMS at varied I_s. Before being loaded into the vacuum chamber, all substrates had been ultrasonically cleaned in acetone and alcohol. Then, the vacuum chamber was pumped down to a base pressure of 2×10^{-3} Pa and the substrates were heated up to 300 °C. During the film deposition process, the bias voltage of filament was fixed at −80 V and U_s was settled as −100 V, and an individually controllable I_s from 0.1 to 6.0 A can be obtained by adjusting the heating current of filament. The power density of Ti target (99.7% purity) remained constant, nearly 4.0 W/cm². The flow rates of Ar (99.999% purity) and N$_2$ (99.999% purity) were fixed at 60 sccm and 14 sccm, respectively; the total pressure was about 0.6 Pa. The duration of the deposition of TiN film was 120 min. Prior to the deposition of TiN film, the substrates were etched by Ar$^+$ ions for 90 min and a Ti intermediate layer was deposited for 10 min in order to enhance the adhesive strength between the films and their substrates.

The chemical composition of the films was analyzed using an X-ray photoelectron spectroscopy (XPS, PHI Quantera SXM, ULVAC-PHI, Japan) in ultra-high vacuum of 1.33×10^{-5} Pa. A monochromatic Al-Kα radiation (39.9 W) with a pass energy of 280 eV for survey spectra and 55 eV for narrow spectra. The step was 1 eV for survey spectra and 0.1 eV for narrow spectra. The beam spot size and the incidence angle of X-ray were 200 μm and 45°, respectively. Prior to acquiring XPS data, Ar$^+$ ion beam etching was operated with an etching depth of 100 nm to remove the surface contaminations. Peak fitting was performed by XPSPEAK41 software; after a Shirley background subtraction and the peaks were fitted using a non-liner least squares fitting of a mixed Gaussian/Lorentzian product function. The surface and cross-section morphologies of the films were observed by scanning electron microscopy (SEM, JSM-7610FPlus, JEOL, Japan). The operating voltage was 15 kV. Laser confocal microscopy (LEXT OLS5000, Olympus, Japan) was utilized to measure the surface roughness of the coated samples. The phase structure of the films was determined by X-ray diffraction (XRD, D/max 2500, Rigaku, Japan) with Cu Kα radiation in the theta/2theta mode.

The nanohardness and effective Young's modulus of the films were measured by a nanoindenter (Nano Indenter II, MTS, America) in the continuous stiffness mode with a pressed depth of 100 nm, and eight measurements were executed. Scratch tests were conducted with a multifunctional tester for material surface (MFT 4000, Lanzhou Hua Hui Instrument Technology Co., China). The scratch length was 5 mm. The maximum load was 100 N and the loading rate was 100 N/min. Three measurements were operated for each sample.

Tribological tests were carried out against GCr15 counterpart balls (φ6 mm) under dry friction conditions for 30 min with a ball-on-disk tribometer (MST 3001, Lanzhou Hua Hui Instrument Technology Co., China). The typical test conditions were as follows: radius of wear track, 4 mm; rotational speed, 300 r/min; normal load, 5 N. After the tribological tests, the sectional area of the wear tracks on the TiN-coated samples were measured by laser confocal microscopy (LEXT OLS5000, Olympus, Japan) and the wear rates (K) of the samples were calculated using the equation below, according to Forniés et al. [19].

$$K = \frac{A \cdot d}{s \cdot F} \tag{1}$$

Where A are the sectional areas of wear tracks, d are the perimeters of wear tracks, s is sliding distance and F is normal load. The surface morphologies of the wear tracks were observed by SEM (JSM-6510, JEOL, Japan) equipped with an EDS (Genesis XM2, EDAX, America). The operating voltages of SEM and EDS were 15 kV.

3. Results and discussion

3.1. Chemical composition

The chemical composition of the TiN films deposited on Si(100) wafers was measured by XPS, and the chemical composition of the films at different I_s is shown in Fig. 1. When I_s is increased, there is no obvious change in the content of N or Ti, and all the films possess a nearly stoichiometric composition. The N_2 flow rate used in this work was determined according to the critical value of the hysteresis loop so as to sputter Ti target in the transition mode, which benefits the synthesis of stoichiometric TiN, as reported by Fontana and Muzart [20].

According to the XPS Ti 2p spectra shown in Fig. 2, there are mainly three peaks for the deposited films at the binding energies of ∼ 455.1 eV, ∼ 456.9 eV and ∼ 458.4 eV, corresponding to Ti2p 3/2 in TiN phase, TiO_xN_y phase and TiO_2 phase, respectively [21]. And no peak attributed to metallic Ti phase is detected. Ponon et al. [22] indicated that a small quantity of TiO_xN_y and TiO_2 phases in the films are mainly attributed to the residual gas in the vacuum chamber or the impurity in the reactive gas.

3.2. Morphology and deposition rate

Fig. 3 exhibits the SEM photos of the surface and cross-section morphologies of the films deposited on Si(100) wafers at varied I_s. When I_s is 0.1 A, a typical tapered microstructure separated by voids and a facetted surface topography are observed, which is attributed to the relative low energy and poor surface diffusion ability of the film-forming particles condensed on the substrate, according to Mayrhofer et al. [10]. The nucleation rate is low and the crystal prefers nucleating along the incidence direction of the film-forming particles, which usually leads to the growth of crystals with relatively large grain sizes. Yang et al. [23] indicated that the faceted morphology is mainly caused by the low surface density and preferred orientation of the crystal. A faceted topography tends to be observed for the films composed of the B1-NaCl crystals with (111) preferred orientation. As I_s is increased from 0.1 to 1.5 A, the structure is transformed into a dense microstructure. The increase of I_s leads to the enhancement of the mobility and average energy of the film-forming atoms, which is beneficial to the nucleation and interrupts the growth of the tapered crystal. As a result, a decrease in the grain size as well as the densification of the films can be expected, as reported by Mayrhofer et al. [10]. When I_s rises to 3.0 A, the compactness of the film is further improved and a nearly defect-free film is produced. However, some defects appear when I_s is further increased.
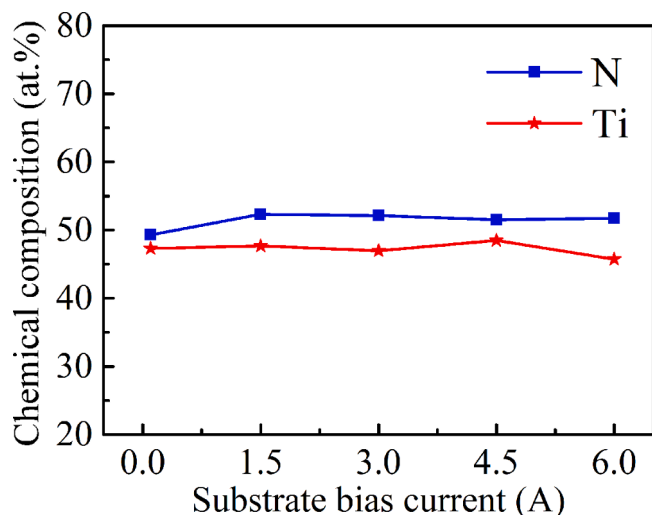
On one hand, the film-forming particles with the enhanced mobility can entry the voids or defects, leading to the densification of the films. On the other hand, when the ion bombardment is excessive, more film-forming particles may be resputtered from the film surface. Moreover, the number of the ions penetrating into the films is also increased, which can cause an increase in the residual stress and defects, as reported by Jiang et al. [21].

It can also be found that the interface between TiN film and Ti intermediate layer becomes more and more ambiguous with increasing I_s. During the deposition process of the Ti intermediate layer, the increased I_s leads to an enhancement of resputtering of the condensed Ti atoms, which brings out a decrease in the thickness of the Ti intermediate layer deposited for a same duration from 60 nm to 25 nm as well as an increase of defects. During the deposition process of TiN film, the number of N_2^+ and N^+ ions is increased as I_s increases. The N_2^+ and N^+ ions may impinge into the forming films and penetrate into the lattices of TiN and Ti, which blurs the interface between Ti intermediate layer and TiN film, similar to the finding of the previous study conducted by He et al. [24].

Fig. 4 illustrates the surface roughness of the TiN films deposited on 40Cr13 stainless steel plates as a function of I_s. When I_s is increased, the surface roughness is decreased at first, but then increased; and the lowest surface roughness of 22 nm is obtained when I_s is 3.0 A. Similar to the evolution of the compactness of the films, there are also two basic and competing processes during the film growth. According to Kong et al. [25], at the stage of a relatively low I_s, the increased ion energy and enhanced diffusion mobility are beneficial to weaken the shadow effect and promote the formation of a smooth surface. However, at the stage of a relatively high I_s, the resputtering effect becomes notable and induces more defects on the surface so that a rough surface is produced, which is in accordance with the investigation conducted by Devia et al. [26].

Fig. 5 shows the deposition rates of the TiN films deposited on Si (100) wafers as a function of I_s. The deposition rates are decreased gradually from 484 to 369 nm/h when I_s is increased from 0.1 to 3.0 A, but the deposition rates shows little dependence on I_s while I_s is further increased. When I_s is increased from 0.1 to 1.5 A, the obvious decrease of the deposition rate is mainly caused by the densification of the deposited films.

3.3. Phase structure

The XRD patterns of the TiN films deposited on Si(100) wafers are shown in Fig. 6. There are mainly five diffraction peaks corresponding to TiN(111), TiN(200), TiN(220), TiN(311) and TiN(222). TiN(111) is dominant diffraction peak almost for all the deposited samples. Under the condition of I_s=1.5 A, the TiN film exhibits random orientation; but when I_s is more or less than 1.5 A, the strong preferred orientation of TiN (111) in the films is shown.

According to Musil [27], in the simplest case of a less collision, the energy delivered to the growing film by conversion of the kinetic energy of bombarding ions (E_s) can be expressed as the equation below:

$$E_s \approx \frac{U_s I_s}{a_D} \tag{2}$$

Where U_s represents the substrate bias voltage, I_s represents the substrate bias current, and a_D represents the deposition rate. It can be found that a pronounced increase of E_s is established as I_s is increased from 0.1 to 1.5 A. And the texture evolution in the films is mainly related to E_s. As is known, the film growth is controlled by its overall energy including interfacial energy, strain energy and surface energy. Zhou et al. [28] demonstrated that due to the mismatch between Si substrate and TiN film, TiN film growth usually follows the Volmer-Weber mode and the interfacial energy has less influence on the formation of the texture of the films. Therefore, the competition between the strain energy and surface energy contributes to the texture evolution of the films with increased I_s. The strain energy (U_{hkl}) terms for the two-dimensional cases with equivalent primary stresses is expressed as the equation

Fig. 1. Chemical composition of TiN films deposited at varied I_s.
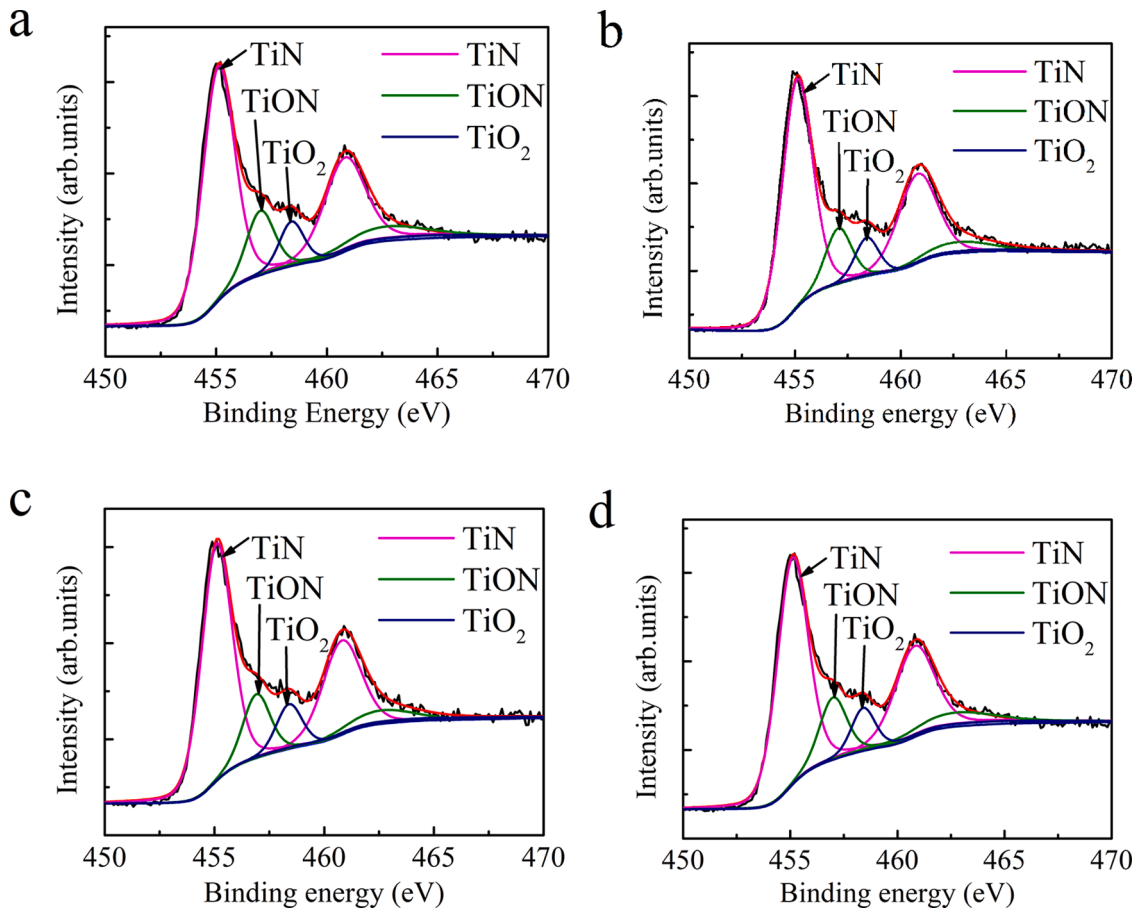
Fig. 2. XPS Ti 2p of TiN films deposited at varied I_s (a) 0.1 A, (b). 1.5 A, (c) 3.0 A, (d) 6.0 A.

below [29]:

$$U_{hkl} = \varepsilon^2 E(1-\nu) \qquad (3)$$

Where ε is the strain in the specific plane of the film, E is the elastic modulus of the specific plane of the film and ν is the Poisson ratio of the films. The surface energy (S_{hkl}) for different orientations can be evaluated by the equation below [29]:

$$S_{hkl} = \frac{6.5 \times 10^{-19} n_{hkl}}{z} \qquad (4)$$

Where n_{hkl} is the number of the broken bonds per square centimeter for the specific planes, z is coordination number. Apelleg et al. [29] found that in B1-typed NaCl structure, TiN(200) plane possesses the lowest surface energy, while TiN(111) plane has the lowest strain energy. When I_s is 0.1 A, the highest deposition rate and porous microstructure can result in larger inner stress, which makes strain energy dominate the preferred orientation of the film, so the preferred orientation of TiN(111) is formed. When I_s approaches 1.5 A, the significantly increased energy and atom mobility of the film-forming particles benefit the release of the inner stress in the film. Therefore, the film deposited at 1.5 A consists of the randomly oriented fine crystals. When I_s is increased from 1.5 to 3.0 A, the average kinetic energy of bombarding ions exceeds a threshold value and results in resputtering and an increased compressive stress, which makes strain energy dominate the preferred orientation of the film again. Hence, an obvious preferred orientation of TiN(111) is obtained. Besides, at a relative high I_s values, TiN(200) plane permits more ions with high energy to entry the crystal lattice or resputter more atoms from it, while the TiN(111) plane is the densest plane, in which the atoms possess the highest adhesive strength and are difficult to be resputtered.

The grain sizes were calculated using Scherrer formula [30]:

$$D = \frac{0.9\lambda}{FWHM cos\theta} \qquad (5)$$

Where D is the grain size along the normal direction of a specific plane, λ is X-ray wavelength, θ is the Bragg angle and $FWHM$ is the corrected full width at half maximum. The grain size corresponding to the TiN(111) is displayed in Fig. 7. As I_s increases from 0.1 to 1.5 A, a distinct reduction in grain size is found; but when I_s is further increased, the grain size is slightly increased. When I_s is increased from 0.1 to 1.5 A, the enhanced atom mobility and nucleation lead to the decrease in the grain size, as Mayrhofer et al. [10] reported. Moreover, according to Chen et al. [8], the increased ion bombardment leads to the interruption of grain growth and induces the increase of dislocations, which prevents the migration of grain boundaries and also helps to decrease the grain size.

3.4. Mechanical properties

Fig. 8 displays the hardness (H) and effective Young's modulus (E^*) of the films deposited on Si(100) wafers as a function of I_s. When I_s is increased from 0.1 to 1.5 A, H and E^* of the films are evidently increased from 12.8 and 254.9 GPa, to 34.5 and 413.9 GPa, respectively; but as I_s is further increased, there is no obvious change in those properties. The significant increase in H and E^* is mainly attributed to the finer and denser microstructure discussed in the Section 3.2 and 3.3, in accordance with the study of He et al. [24]. According to the Hall-Petch relationship, the movement of dislocations and the propagation of cracks along the grain boundaries are significantly restricted as the grain size is decreased, which results in the improved hardness [26]. Additionally, the significantly enhanced hardness at 1.5 A may be also
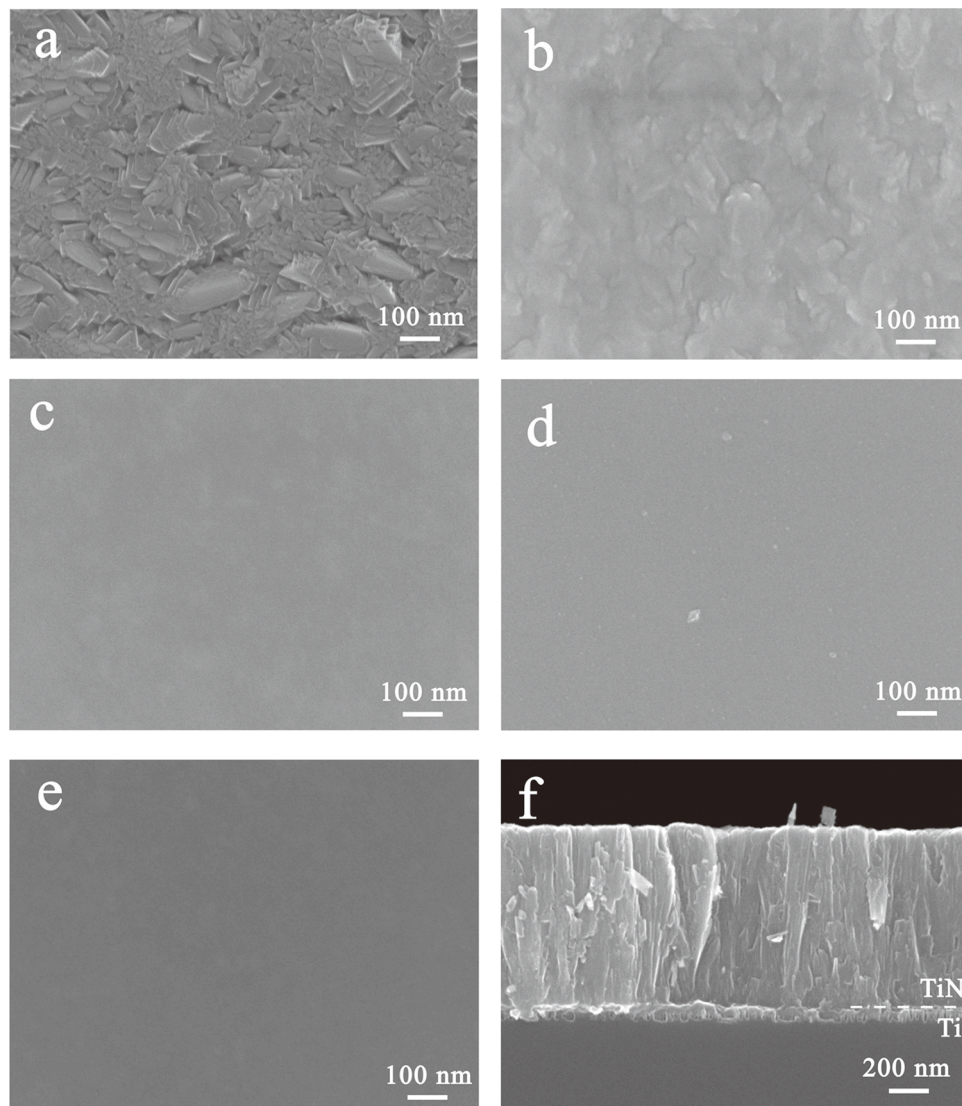
Fig. 3. SEM photos of surface and cross-section morphologies of TiN films deposited at different I_s (a, f) 0.1 A, (b, g) 1.5 A, (c, h) 3.0 A, (d, i) 4.5 A, (e, j) 6.0 A.

related to the random orientation of the films as well, which results in the increase of the phase boundaries and grain boundaries enhancing the films' hardness, as indicated by Musil [27]. Besides, According to Lin et al. [31], TiN(111) possesses the highest hardness among the crystal orientations of TiN since the Schmid factor of the slip system for the (111) crystal plane of TiN is zero. So the apparent TiN(111) preferred growth helps the films maintain high hardness, when I_s exceeds 3.0 A.

Jaroš et al. [9] reported that H/E^* and H^3/E^{*2} ratios are inferred to the resistance to cracking and the resistance to plastic deformation of the films, respectively. It has been found by Leyland and Matthews [32] that the higher H/E^* and H^3/E^{*2} ratios are the intimations of better wear resistance. Fig. 9 presents the H/E^* and H^3/E^{*2} ratios as a function of I_s. When I_s is increased from 0.1 to 1.5 A, H/E^* and H^3/E^{*2} ratios are evidently improved; but as I_s is further increased, H/E^* and H^3/E^{*2} ratios show less dependence on I_s. The variations of H/E^* and H^3/E^{*2} ratios as functions of I_s are similar to those of the hardness and the effective Young's modulus. The improvements of H/E^* and H^3/E^{*2} ratios are mainly attributed to the fine grain size as discussed above. The highest H/E^* and H^3/E^{*2} ratios are obtained at 3.0 A, indicating that the best wear resistance may be obtained when I_s is 3.0 A.

The critical load (L_c) obtained from the scratch test is the load which is related to the location of chipping point for the films and used to

characterize the adhesive strength between the films and their substrates, according to Chen et al. [8]. Fig. 10 presents the variation of L_c of the TiN-coated 40Cr13 stainless steel samples with the increase of I_s. When I_s is increased from 0.1 to 1.5 A, L_c is decreased from 61.0 to 50.5 N; but with the further increase of I_s, L_c is nearly unchanged. The decline in the adhesive strength is possibly due to the decrease in the thicknesses of the Ti intermediate layers. The study conducted by Bushroa et al. [33] shown that adhesive strength between the film and the steel substrate benefits from the existence of Ti intermediate layer for its good metallicity and ductility. As it can be seen from Fig. 3, the highest L_c at 0.1 A is mainly because of its largest thickness of the Ti intermediate layer. When I_s is increased from 1.5 to 6.0 A, the denser microstructure and enhanced H/E^* and H^3/E^{*2} ratios are conducive to prevent the delamination of the films and a relatively good adhesive strength above 48 N is obtained in the whole range of I_s.

3.5. Tribological properties

Fig. 11 presents the friction coefficients and wear rates of the TiN-coated 40Cr13 stainless steel samples against GCr15 counterpart balls. The friction coefficients of the TiN-coated 40Cr13 stainless steel samples at the steady wear stage are varied from 0.50 to 0.56, and the effect of I_s
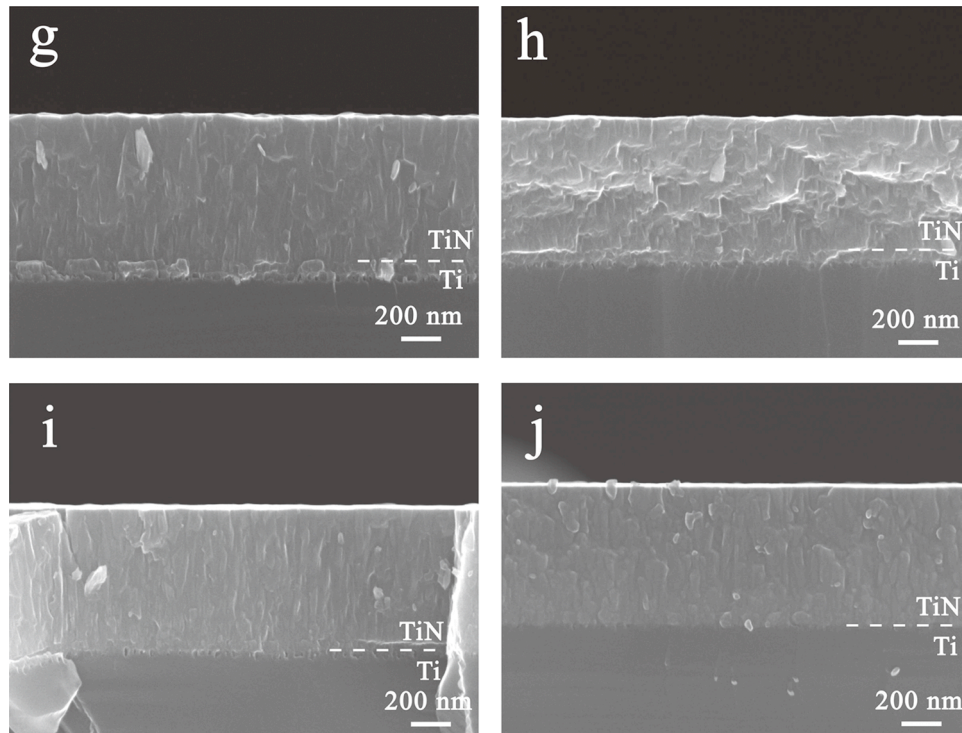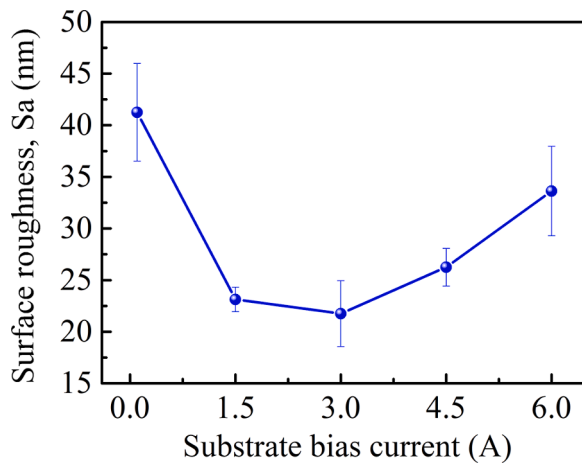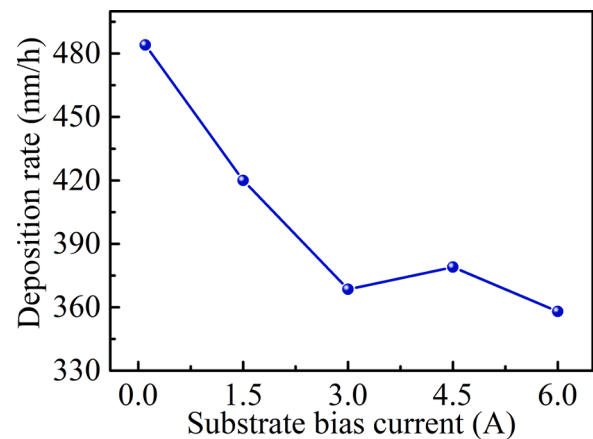
Fig. 3. (*continued*).

Fig. 4. Surface roughness (Sa) of TiN films as function of I_s.

Fig. 5. Deposition rates of TiN films as function of I_s.

on the friction coefficients is unobvious. When I_s is increased from 0.1 to 3.0 A, the wear rates of the TiN-coated samples are obviously decreased whereas the wear rates are gradually increased as I_s further increases; and the lowest wear rate of 9.4×10^{-16} m^3/(N•m) is obtained when I_s is 3.0 A. Similar to the results that Yeh et al. [34] observed, the distinct improvement of the compactness and the highest hardness as well as the highest H/E^* and H^3/E^{*2} ratios contribute to the best wear resistance, when the TiN-coated samples prepared at 3.0 A. Additionally, the best wear resistance is also correlated to the lowest surface roughness of the sample produced at 3.0 A.

Fig. 12 displays the topographs of the wear tracks on the TiN-coated 40Cr13 stainless steel samples prepared at various I_s, and the insets are the enlarged morphological photos of the wear tracks for the same sample. The breadth of the wear tracks on the TiN-coated samples is first decreased, but then increased, which is consistent with the variation of the wear rate. According to the results of EDS analysis of the selected areas in the wear tracks referred to Fig. 12 (listed in Table 1), there are three main metallic elements including Ti, Cr and Fe existing in the wear tracks. Ti comes from the TiN films, while Cr and Fe come from the 40Cr13 stainless steel substrates.

According to the EDS analysis of area 2, the apparent increase in Fe, Cr, O content and decrease in N, Ti content for the center zone of the worn scars is found when compared with the composition of the unworn zone (area 1), which indicates the severe peeling of TiN films. For the TiN-coated sample prepared at I_s of 0.1 A, because of the loose microstructure and low hardness of the film, GCr15 counterpart ball is pressed deeply into the film and causes stress concentration at the interface between the film and its substrate. So, the contact area is apt to be deformed plastically and welded together. When the contact zones of the counterparts are separated during wear process, the welded junction is broken and the film peels off from the substrate. Therefore, a large area of peeling with a great depth is observed. In the wear track of the TiN-coated sample prepared at I_s of 0.1 A, some fine oxide particles are also observed, which means besides the serious adhesive wear, oxidative
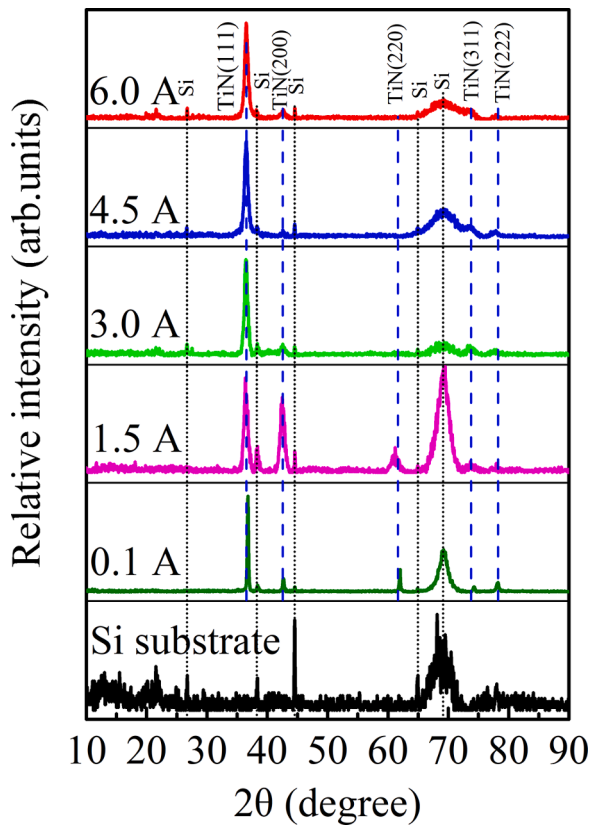
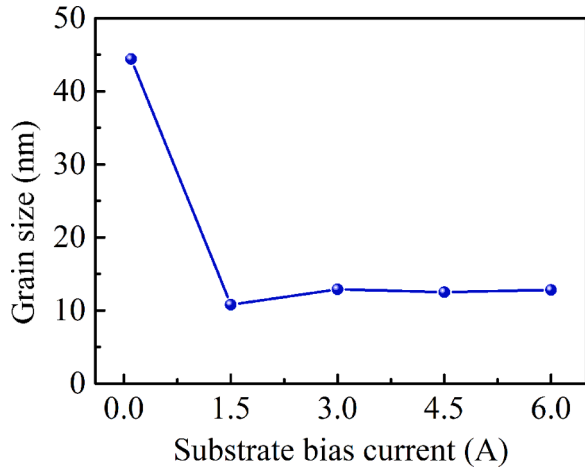**Fig. 6.** XRD patterns of TiN films deposited at different I_s.

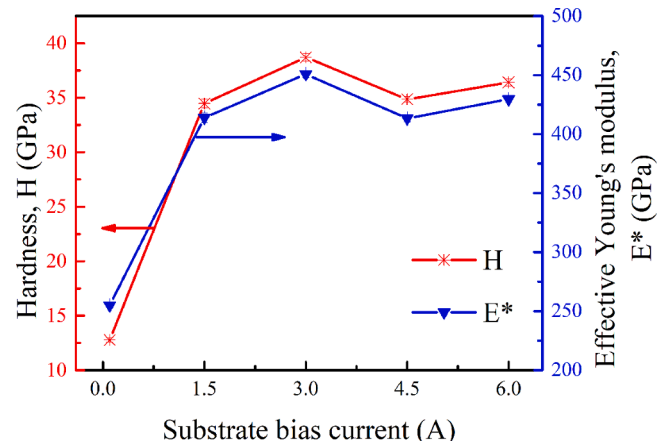**Fig. 7.** Grain sizes of TiN films deposited at varied I_s.

Fig. 8. Hardness and effective Young's modulus of TiN films versus I_s.
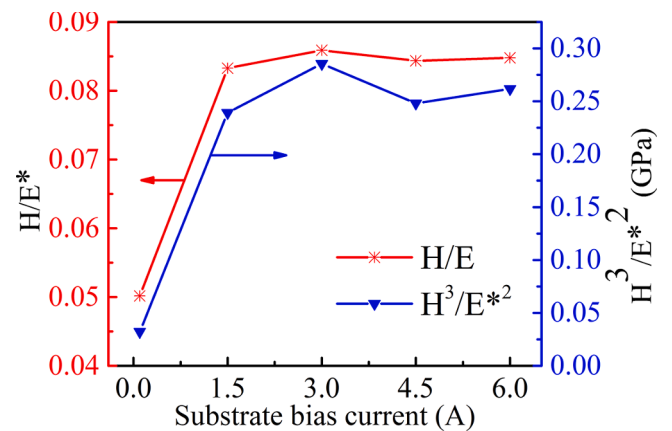
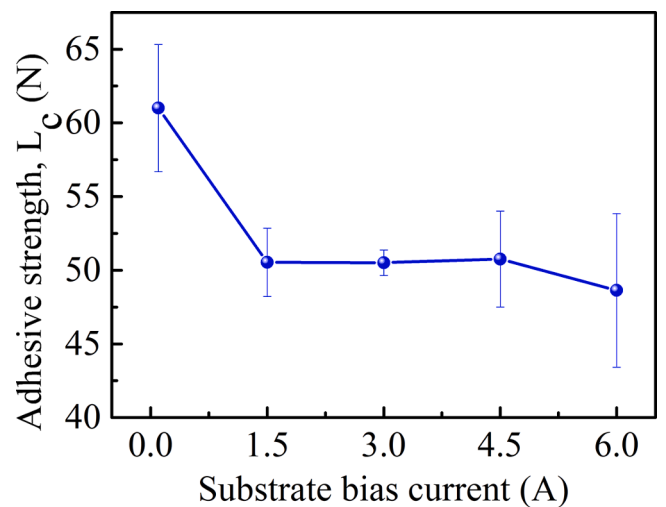**Fig. 9.** H/E^* and H^3/E^{*2} of TiN films versus I_s.

Fig. 10. Adhesive strength of TiN films versus I_s.

wear also happens. The film is easily oxidized due to its loose microstructure and high density of defects. Additionally, the debris may become hard abrasive particles in the wear track due to the oxidation and work-hardening, which further aggravates the wear of the TiN-coated sample.

When I_s is increased to 1.5 A, according to the EDS analysis results of area 3 and 4, spallation and peeling also clearly appears. However, due to the improved mechanical properties and fine microstructure of the TiN film, the plastic deformation of the film is evidently limited, and the stress concentration is confined to the contact area or inside the counterpart ball, so that the peeling of the films is decreased and its depth is also effectively restricted. Thus, the failure of the coated samples is mainly caused by the adhesive wear and fatigue wear. When I_s is 3.0 A,

based on the EDS analysis results of area 6 and its morphology, plastic deformation and material transfer occurs when the relatively soft GCr15 counterpart ball contacts with the hard TiN-coated sample under normal load. And then the stress was accumulated near the asperities on the surface of the sample under the cyclic stress during the wear process, which promotes the initiation and propagation of the cracks and leads to the chipping of the films (area 7). When I_s is further increased to more
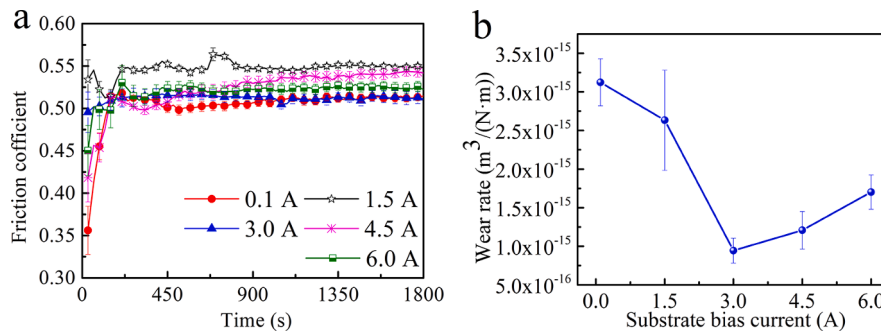
Fig. 11. Friction coefficients (a) and wear rates (b) of TiN-coated samples obtained at different I_s.
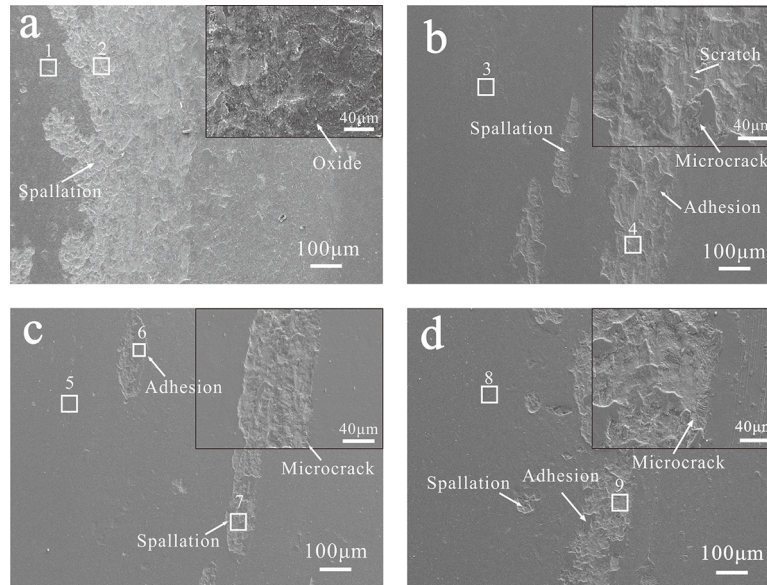

Fig. 12. SEM photos of topographies of wear tracks of TiN-coated samples prepared at various I_s (a) 0.1 A, (b) 1.5 A, (c) 3.0 A, (d) 6.0 A. Detailed EDS analysis results of areas 1–9 are presented in Table 1.

Table 1
EDS analysis results of selected areas in wear tracks of TiN-coated samples prepared at varied I_s (at.%). Areas 1–9 are marked in Fig. 12.

Area	0.1 A (Fig. 12a)		1.5 A (Fig. 12b)		3.0 A (Fig. 12c)			6.0 A (Fig. 12d)	
	1	2	3	4	5	6	7	8	9
N	25	6	24	0	25	0	19	20	0
O	19	23	5	0	5	48	15	0	10
Ti	43	8	55	5	51	8	27	54	10
Cr	2	8	3	13	3	2	6	4	11
Fe	11	55	14	82	16	42	33	21	70

than 3.0 A, since the excessive ion bombardment, besides the adhesion (area 8), the increased residual stress and defects in the films and at the interfaces may further promote the formation and propagation of the microcracks, which causes serious delamination (area 9). Therefore, the wear resistance of the samples is gradually weakened. Moreover, the reappearance of the scratches is probably related to the increased debris and the increased surface roughness.

4. Conclusions

I_s has a great impact on the microstructure and properties of TiN films deposited by PEMS. The TiN films with a nearly stoichiometric composition are produced in the whole range of I_s. When I_s is increased from 0.1 to 3.0 A, the compactness of the TiN films is improved. As I_s is increased from 0.1 to 1.5 A, a transformation of the preferred orientation of TiN film from TiN(111) to a mixture of TiN(111) and TiN(200) is obtained and the grain sizes in the films are distinctly reduced. However, with further increasing I_s, the preferred orientation of the films is changed to TiN(111) again. When I_s is increased from 0.1 to 1.5 A, the hardness and effective Young's modulus of the films are greatly improved while the adhesive strength is slightly decreased. With increasing I_s, the wear rates of the TiN-coated samples are distinctly decreased at first, but then gradually increased; and the lowest wear rate of 9.4×10^{-16} m^3/(N•m) is obtained when I_s is 3.0 A.

References

[1] A.R. Machado, L.R.R. da Silva, F.C.R. de Souza, R. Davis, L.C. Pereira, W.F. Sales, W. de Rossi, E.O. Ezugwu, State of the art of tool texturing in machining, J. Mater. Process. Tech. 293 (2021), 117096, https://doi.org/10.1016/j.jmatprotec.2021.117096.

[2] L. Hacisalihoglu, F. Yildiz, A. Alsaran, Wear performance of different nitride-based coatings on plasma nitrided AISI M2 tool steel in dry and lubricated conditions, Wear 384-385 (2017) 159–168, https://doi.org/10.10.16/j.wear.2017.01.17.

[3] Y.H. Celik, E. Kilickap, M. Guney, Investigation of cutting parameters affecting on tool wear and surface roughness in dry turning of Ti-6Al-4V using CVD and PVD coated tools, J Braz. Soc. Mech. Sci. Eng. 39 (2017) 2085–2093, https://doi.org/10.1007/s40430-016-0607-6.

[4] M. Tkadletz, C. Mitterer, B. Sartory, I. Letofsky-Papst, C. Czettl, C. Michotte, The effect of droplets in arc evaporated TiAlTaN hard coatings on the wear behavior, Surf. Coat. Tech. 257 (2014) 95–101, https://doi.org/10.1016/j.surfcoat.2014.01.010.

[5] Z.G. Zhang, O. Rapaud, N. Bonasso, D. Mercs, C. Dong, C. Coddet, Control of microstructures and properties of dc magnetron sputtering deposited chromium nitride films, Vacuum. 82 (2008) 501–509. http://doi:10.1016/j.vacuum.2007.08.009.

[6] B. Biswas, Y. Purandare, A. Sugumaran, I. Khan, P.E. Hovsepian, Effect of chamber pressure on defect generation and their influence on corrosion and tribological properties of HIPIMS deposited CrN/NbN coatings, Surf. Coat. Tech. 336 (2018) 84–91, https://doi.org/10.1016/j.surfcoat.2017.08.021.

[7] P.H. Mayrhofer, G. Tishler, C. Mitterer, Microstructure and mechanical/thermal properties of Cr-N coatings deposited by reactive unbalanced magnetron sputtering, Surf. Coat. Tech. 142-144 (2001) 78–84, https://doi.org/10.1016/S0257-8972(01)01090-8.

[8] X. Chen, Y.T. Xi, J. Meng, X.L. Pang, H.S. Yang, Effects of substrate bias voltage on mechanical properties and tribological behaviors of RF sputtered multilayer TiN/CrAlN films, J. Alloy. Compd. 665 (2016) 210–217, https://doi.org/10.1016/j.jallcom.2015.10.076.

[9] M. Jaroš, J. Musil, R. Čerstvý, S. Haviar, Effect of energy on structure, microstructure and mechanical properties of hard Ti(A,V)N$_x$ films prepared by magnetron sputtering, Surf. Coat. Tech. 332 (2017) 190–197, https://doi.org/10.1016/j.surfcoat.2017.06.074a.

[10] P.H. Mayrhofer, F. kunc, J. Musil, C. Mitterer, A comparative study on reactive and non-reactive unbalanced magnetron sputter deposition of TiN coatings, Thin Solid Films 415 (2002) 151–159, https://doi.org/10.1016/S0040-6090(02)00511-4.

[11] J. Lin, Z.L. Wu, X.H. Zhang, B. Mishra, J.J. Moore, W.D. Sproul, A comparative study of CrN$_x$ coatings Synthesized by dc and pulsed dc magnetron sputtering, Thin Solid Films 517 (2009) 1887–1894, https://doi.org/10.1016/j.tsf.2008.09.093.

[12] Q.S. Ma, L.H. Li, Y. Xu, J.B. Gu, L. Wang, Y. Xu, Effect of bias voltage on TiAlSiN nanocomposite coatings deposited by HiPIMS, Appl. Surf. Sci. 392 (2017) 826–833, https://doi.org/10.1016/j.apsusc.2016.09.028.

[13] J. Matossian, R.H. Wei, J. Vajo, G. Hunt, M. Gardos, G. Chambers, L. Soucy, D. Oliver, L. Jay, M. Taylor, G. Alderson, R. Komanduri, A. Perry, Plasma-enhanced, magnetron-sputtered deposition (PMD) of materials, Surf. Coat. Tech. 108-109 (1998) 496–506, https://doi.org/10.1016/S0257-8972(98)00632-X.

[14] A.M.A. El-Rahman, R.H. Wei, A comparative study of conventional magnetron sputter deposited and plasma enhanced magnetron sputter deposited Ti–Si–C–N nanocomposite coatings, Surf. Coat. Tech. 241 (2014) 74–79, https://doi.org/10.1016/j.surfcoat.2013.08.049.

[15] R.H. Wei, J.J. Vajo, J.N. Matossian, M.N. Gardos, Aspects of plasma-enhanced magnetron-sputtered deposition of hard coatings on cutting tools, Surf. Coat. Tech. 158-159 (2002) 465–472, https://doi.org/10.1016/S0257-8972(02)00289-Xa.

[16] A.M.A. El-Rahman, R.H. Wei, Effect of ion bombardment on structural, mechanical, erosion and corrosion properties of Ti–Si–C–N nanocomposite coatings, Surf. Coat. Tech. 258 (2014) 320–328, https://doi.org/10.1016/j.surfcoat.2014.09.006.

[17] C. Lorenzo-Martin, O. Ajayi, A. Erdemir, G.R. Fenske, R.H. Wei, Effect of microstructure and thickness on the friction and wear behavior of CrN coatings, Wear 302 (2013) 963–971, https://doi.org/10.1016/j.wear.2013.02.005.

[18] F. Cai, X. Huang, R.H. Wei, D. Nagy, Microstructure and tribological properties of CrN and CrSiCN coatings, Surf. Coat. Tech. 205 (2010) 182–188, https://doi.org/10.1016/j.surfcoat.2010.06.033.

[19] E. Forniés, R.Escobar Galindo, O. Sánchez, J.M. Albella, Growth of CrN$_x$ films by DC reactive magnetron sputtering at constant N$_2$/Ar gas flow, Surf. Coat. Tech. 200 (2006) 6047–6053, https://doi.org/10.1016/j.surfcoat.2005.09.020.

[20] L.C. Fontana, J.L.R. Muzart, Triode magnetron sputtering TiN film deposition, Surf. Coat. Tech. 114 (1999) 7–12, https://doi.org/10.1016/S0257-8972(99)00032-8.

[21] N. Jiang, H.J. Zhang, S.N. Bao, Y.G. Shen, Z.F. Zhou, XPS study for reactively sputtered titanium nitride thin films deposited under different substrate bias, Physica B 352 (2004) 118–126, https://doi.org/10.1016/j.physb.2004.07.001.

[22] N.K. Ponon, D.J.R. Appleby, P.J.King E.Arac, S. Ganti, S.K. Kwa, A. O'Neill, Effect of deposition conditions and post deposition anneal on reactively sputtered titanium nitride thin films, Thin Solid Films 578 (2015) 31–37, https://doi.org/10.1016/j.tsf.2015.02.009.

[23] K. Yang, J.Q. Liang, M.Y. Gu, Effects of nitrogen partial pressure on microstructure, morphology and N/Ti ratio of TiN films deposited by reactive magnetron sputtering, Mater. Sci. Tech. 23 (2007) 958–962, https://doi.org/10.1179/174328407X192859.

[24] C.L. He, J.L. Zhang, G.F. Ma, Z.F. Du, J.M. Wang, D.L. Zhao, Influence of bias voltage on structure, mechanical and corrosion properties of reactively sputtered nanocrystalline TiN films, J. Iron. Steel. Res. Int. 24 (2017) 1223–1230, https://doi.org/10.1016/S1006-706X(18)30021-9.

[25] Q.H. Kong, J. Ji, H.X. Li, X.H. Liu, Y.J. Wang, J.M. Chen, H.D. Zhou, Influence of substrate bias voltage on the microstructure and residual stress of CrN films deposited by medium frequency magnetron sputtering, Mater. Sci. Eng. B-Adv. Funct. Solid-State Mater. 176 (2011) 850–854, https://doi.org/10.1016/j.mseb.2011.04.015.

[26] D.M. Devia, E. Restrepo-Parra, J.Arango P, A.P. Tschiptschin, J.M. Velez, TiAlN coatings deposited by triode magnetron sputtering varying the bias voltage, Appl. Surf. Sci. 257 (2011) 6181–6185, https://doi.org/10.1016/j.apsusc.2011.02.027.

[27] J. Musil, Hard nanocomposite coatings: thermal stability, oxidation resistance and toughness, Surf. Coat. Tech. 207 (2012) 50–65, https://doi.org/10.1016/j.surfcoat.2012.05.073.

[28] T. Zhou, D.W. Liu, Y. Zhang, T.Y. Ouyang, J.P. Suo, Microstructure and hydrogen impermeability of titanium nitride thin films deposited by direct current reactive magnetron sputtering, J. Alloy. Compd. 688 (2016) 44–50, https://doi.org/10.1016/j.jallcom.2016.06.278.

[29] J. Apelleg, L.Z. Zevin, S. Lungo, Reactive-sputter-deposited TiN films on glass substrates, Thin Solid Films 197 (1991) 117–128, https://doi.org/10.1016/0040-6090(91)90225-M.

[30] H.M. Shah, R. Jayaganthan, D. Kaur, Effect of sputtering pressure and temperature on DC magnetron sputtered CrN films, Surf. Eng. 26 (2013) 629–637, https://doi.org/10.1179/174329409X389326.

[31] Y.W. Lin, C.W. Lu, G.P. Yu, J.H. Huang, Structure and properties of nanocrystalline (TiZr)$_x$N$_{1-x}$ thin films deposited by DC unbalanced magnetron sputtering, J. Nanomater. 2016 (2016) 1–12, https://doi.org/10.1155/2016/2982184.

[32] A. Leyland, A. Matthews, On the significance of the H/E ratio in wear control: a nanocomposite coating approach to optimised tribological behaviour, Wear 246 (2000) 1–11, https://doi.org/10.1016/S0043-1648(00)00488-9.

[33] A.R. Bushroa, H.H. Masjuki, M.R. Muhamad, B.D. Beake, Optimized scratch adhesion for TiSiN coatings deposited by a combination of DC and RF sputtering, Surf. Coat. Tech. 206 (2011) 1837–1844, https://doi.org/10.1016/j.surfcoat.2011.07.

[34] T.S. Yeh, J.M. Wu, L.J. Hu, The properties of TiN thin films deposited by pulsed direct current magnetron sputtering, Thin Solid Films 516 (2008) 7294–7298, https://doi.org/10.1016/j.tsf.2008.01.001.